Research Article | Open Access

Microstructures

Liu et al. Microstructures 2026, 6, 2026025 DOI:10.20517/microstructures.2025.37

Electrically tunable transmissive dielectric metamaterial based on $SrTiO_3$ Mie resonators

Lanqi Liu[1,2,#], Xiaobo Wang[3,#], Yichen Wang[3], Runni Zhao[1], Yue Jin[3], Bo Li[2,4], Yongzheng Wen[1], Ji Zhou[1]

Keywords: Metamaterial, electrically tunable, transmission, Mie resonance

Citation: Liu, L.; Wang, X.; Wang, Y.; Zhao, R.; Jin, Y.; Li, B.; Wen, Y.; Zhou, J. Electrically tunable transmissive dielectric metamaterial based on $SrTiO_3$ Mie resonators. *Microstructures* **2026**, *6*, 2026025. https://dx.doi.org/10.20517/microstructures.2025.37

Received: 20 Mar 2025 **First Decision:** 27 May 2025 **Revised:** 11 Jun 2025 **Accepted:** 19 Jun 2025 **Published:** 5 Mar 2026

Academic Editor: Shujun Zhang **Copy Editor:** Fangling Lan **Production Editor:** Fangling Lan

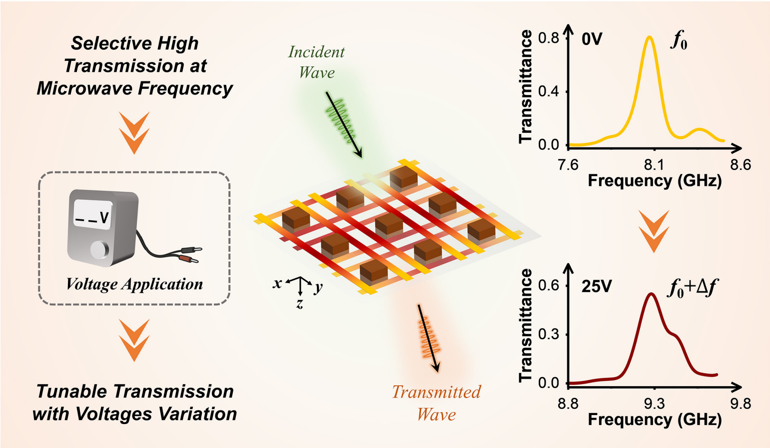

Abstract

Metamaterials have become an important strategy for enhancing electromagnetic wave transmission, and the realization of transmission tunability has attracted considerable attention in current scientific research. In this study, we propose a transmissive metamaterial consisting of periodically arranged $SrTiO_3$ ceramic particles array and metallic grid array. Taking advantage of the Mie resonance of the dielectric particle array, the dispersion characteristics at the interface are precisely tailored, resulting in high transmission in the microwave frequency range. Furthermore, the temperature-sensitive permittivity of $SrTiO_3$ enables dynamic tuning of the transparency window toward higher frequencies through electrically induced thermal modulation. Both the selective high-transmissive performance and electrical tunability are validated through numerical simulations and experimental measurements. This work provides a convenient route to design tunable metamaterials, offering fascinating possibilities for the development of active microwave windows.

[1]State Key Laboratory of New Ceramic Materials, School of Materials Science and Engineering, Tsinghua University, Beijing 100084, China.
[2]Tsinghua Shenzhen International Graduate School, Tsinghua University, Shenzhen 518055, Guangdong, China.
[3]Research Center of Metamaterials, Wuzhen Laboratory, Jiaxing 314500, Zhejiang, China.
[4]Suzhou Laboratory, Suzhou 215123, Jiangsu, China.
[#]Authors contributed equally.

Correspondence to: Prof. Bo Li, Tsinghua Shenzhen International Graduate School, Tsinghua University, No. 2279, Lishui Road, Shenzhen 518055, Guangdong, China; Suzhou Laboratory, No. 388, Ruoshui Road, Suzhou 215123, Jiangsu, China. E-mail: boli@mail.tsinghua.edu.cn; Prof. Yongzheng Wen, State Key Laboratory of New Ceramic Materials, School of Materials Science and Engineering, Tsinghua University, No. 30, Shuangqing Road, Beijing 100084, China. E-mail: wenyzheng@tsinghua.edu.cn; Prof. Ji Zhou, State Key Laboratory of New Ceramic Materials, School of Materials Science and Engineering, Tsinghua University, No. 30, Shuangqing Road, Beijing 100084, China. E-mail: zhouji@tsinghua.edu.cn

INTRODUCTION

Electromagnetic wave transmission has found extensive applications across diverse domains, including wireless communications, radar systems, broadcasting technologies, and microwave remote sensing. The enhancement of transmission constitutes a critical research frontier in electromagnetic wave engineering. Conventional materials are inherently incapable of achieving selective transmission and dynamic modulation. Metamaterials, as an artificial material system capable of electromagnetic wave manipulation, have emerged as a promising solution for transmissive structures. They are artificially designed materials composed of subwavelength structures arranged in specific configurations. Due to the structural design flexibility, metamaterials can exhibit exotic electromagnetic properties unattainable in nature[1-4], and have therefore been applied to numerous novel applications including perfect absorption[5,6], electromagnetic cloaking[7,8], and polarization control[9]. Based on these extraordinary properties and applications, metamaterials are widely used to achieve high transmission, primarily realized through the customized interface dispersion enabled by the specific responses of resonant structures[10,11]. However, conventional metallic resonators exhibit limitations in dynamic modulation under external fields, which has motivated the exploration of tunable methods for dielectric alternatives. Dielectric properties of ceramics are sensitive to external fields, such as heat, static electric, and magnetic fields[12-14], making them promising candidates for constructing active metamaterials.

Methods for actively tuning dielectric metamaterials commonly include electrical and thermal ones. Electrical tunability offers obvious conveniences in practical applications, which can be achieved by integrating with ferroelectric ceramics[15]. By applying the external voltages, the microwave permittivity of the ferroelectric ceramics varies, leading to the shift of the resonant behavior of metamaterials[16,17]. However, such tunability usually requires a large electric field, and its extensions to high-frequency microwave signals are limited due to slow responses of the ferroelectric domain. Temperature field is also one of the external fields to realize tunable performance in metamaterials[18-20]. Based on temperature-dependent characteristics of dielectric materials, thermally tunable metamaterials overcome the limitations of low cutoff frequency, thus enabling their operation to higher frequencies. Nevertheless, achieving precise thermal control on dielectric materials in a compact manner remains challenging.

In this work, we propose a high-transmission metamaterial composed of a ceramic particle array and a metallic grid array, which can be electrically controlled. By applying the external electrical voltage, the metallic grids heated the ceramic particles, which further shifts the resonant behavior of the metamaterials. This results in evident modulations of microwave transmission and frequency selectivity. This method combines the advantages of electrical and thermal tunability, which enables operation in a wider frequency range for the metamaterial and enhances the application feasibility of external fields.

MATERIALS AND METHODS

Mie resonance of dielectric particles provides a practical mechanism for special electromagnetic response in high frequencies. As described by Mie Resonance Theory[21], the effective permittivity (ε_{eff}) and permeability (μ_{eff}) for high-permittivity spherical particles embedded in a low ε matrix are governed by:

$$\varepsilon_{eff} = \varepsilon_1 \left(1 + \frac{3v}{\frac{F(\theta)+2K_e}{f(\theta)-K_e} - v}\right) \tag{1}$$

$$\mu_{eff} = \mu_1 \left(1 + \frac{3v}{\frac{F(\theta)+2K_m}{F(\theta)-K_m} - v}\right) \tag{2}$$

$$F(\theta) = \frac{2(\sin\theta - \theta\cos\theta)}{(\theta^2-1)\sin\theta + \theta\cos\theta} \tag{3}$$

where ε_1, μ_1, and r are the relative permittivity, relative permeability, and radius of the spherical dielectric particles, ε_2 and μ_2 are the relative permittivity and relative permeability of the surrounding medium, respectively. $K_e = \varepsilon_2/\varepsilon_1$, $K_m = \mu_2/\mu_1$, $\theta = k_0 r\sqrt{\varepsilon_1\mu_1}$, where k_0 is the free-space wave number. p is the lattice constant of the structure, and $v = 4\pi^3/3p^3$ represents the volume fraction of the dielectric spheres. Equations (1 and 2) reveal that effective permittivity and permeability can be negative at some θ, so that high-permittivity dielectric particles can be used to construct metamaterials and obtain special electromagnetic response. Among various dielectric ceramics, strontium titanate ($SrTiO_3$), a paraelectric ceramic material at room temperature, demonstrates exceptional intrinsic properties, including high relative permittivity (~300) and low dielectric loss ($\tan\delta < 0.005$). According to the formula of the first-order Mie resonance frequency for spherical particles $f \simeq c/(2r\sqrt{\varepsilon_2})$[10], $SrTiO_3$ particles with a relative permittivity of about 300 resonate in the X-band when fabricated at millimeter-scale dimensions, which can be easily processed. Meanwhile, ceramics with low dielectric loss are preferred in material selection, as ceramics with low loss facilitate the generation of strong resonance inside the particles, which is beneficial to high transmittance. Meanwhile, the resonance frequency of $SrTiO_3$ particles can be tuned to higher frequencies by reducing their sizes. Thus, $SrTiO_3$ was selected to construct our metamaterial. Meanwhile, to simplify the fabrication, cubes rather than spheres were used as the dielectric particles in the metamaterial. Extensive studies have demonstrated that the first-order Mie resonance frequency f of cubic particles with relative permittivity ε_{sp} is governed by an approximately inversely correlated relationship $f \propto 1/\sqrt{\varepsilon_{sp}}$ [11], which is similar to spherical particles.

Figure 1A demonstrates the core elements of the metamaterial and the basic transmissive strategy. The metamaterial integrates a cubic $SrTiO_3$ particle array with a metallic grid array, where the high transmission arises from tailoring interface dispersion through Mie resonance induced by the ceramic particles, coupled with the reflective properties of the metallic structure. Specifically, at the first-order Mie resonance frequency of $SrTiO_3$ ceramics with a relative permittivity of about 300, the ceramic particle array generates a transmission dip. Concurrently, metallic components exhibit intrinsic reflectivity due to their skin depth being orders of magnitude smaller than the thickness. Thus, we strategically designed the phase of reflected fields produced by two types of components to satisfy the destructive interference condition, thereby achieving selective high transmission. The high-transmission mechanism will be detailed in the RESULTS AND DISCUSSION.

The electrically tunable metamaterial is realized by using the temperature-dependent permittivity in ceramic materials. For $SrTiO_3$, the relationship between temperature and its relative permittivity can be approximately expressed by the formula[22]:

$$\frac{1}{\varepsilon(T)} - \frac{1}{\varepsilon(T_0)} \approx (T - T_0) \times 10^{-5} \tag{4}$$

where $\varepsilon(T_0)$ and $\varepsilon(T)$ represent the relative permittivity of the material at the temperature T_0 and T, respectively. Given the inversely correlated relationship between the first-order Mie resonance frequency and

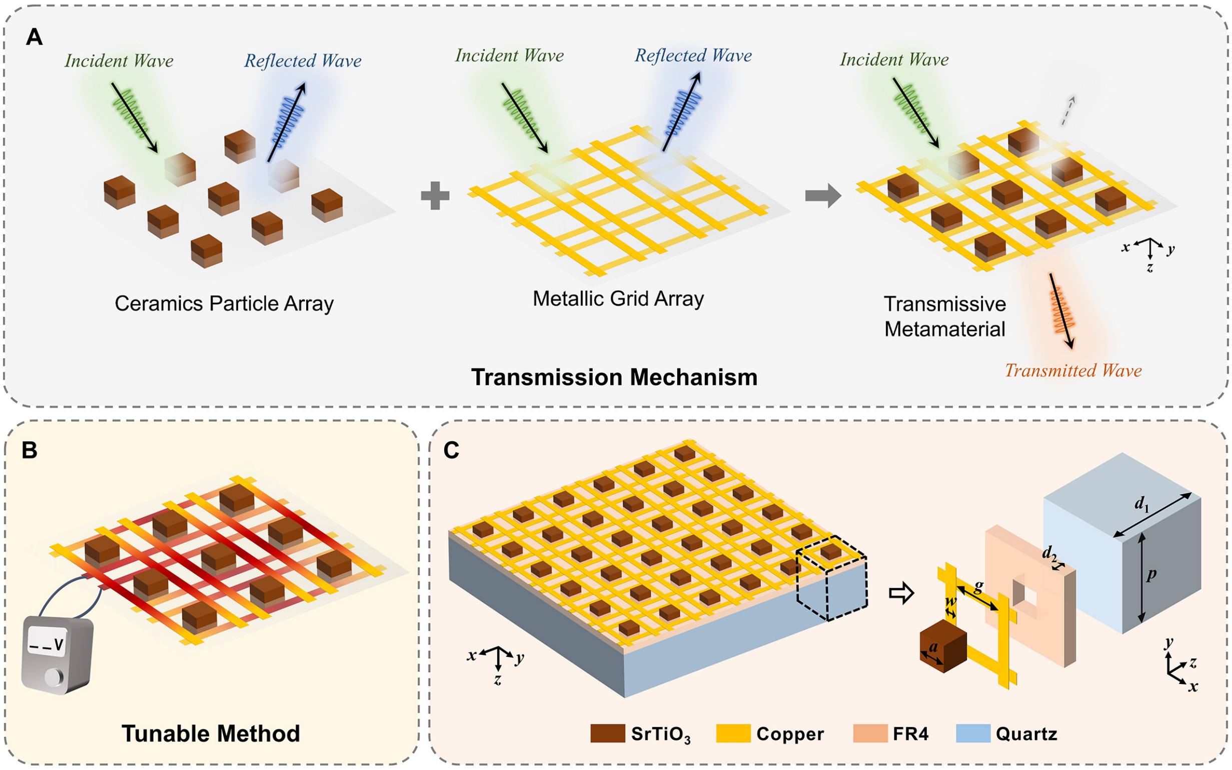

Figure 1. (A) Conceptual schematic diagram of the transmissive mechanism based on destructive interference of dual reflected waves. (B) Conceptual schematic diagram of the practical electrically tuning method. (C) Schematic diagram of the proposed selective high-transmissive metamaterial and dimension annotations of its unit cell.

the relative permittivity of the ceramic material, this relationship depicts that as the temperature increases, the relative permittivity of $SrTiO_3$ decreases, leading to an increase in the resonance frequency. The practical tuning method is applying a voltage to the metallic grid array [Figure 1B], utilizing the thermal effect of the current to heat the ceramic particles located at the center of the unit cell. By applying various voltages, different amounts of heat induced by the current are generated, resulting in different temperature increments. In addition, it should be noted that σ of metal also exhibits a temperature-dependent decrease. However, its absolute magnitude remains sufficiently high to ensure negligible impact on the electromagnetic response.

Based on the aforementioned principles of high transmittance and tunability, we propose a practically fabricable metamaterial structure, as illustrated in Figure 1C, which is composed of periodically arranged $SrTiO_3$ ceramic cubic particles and a metallic grid array. Each cubic particle has a side length of a = 1.8 mm and sets relative permittivity ε = 280, tanδ = 0.0025 as simulation parameters. Copper with a conductivity $\sigma = 5.96 \times 10^7$ S/m and width w = 0.8 mm is selected for the metallic component. The metal structure features a dual-layer configuration with orthogonally aligned horizontal and vertical grids, separated by a polyimide (PI) dielectric interlayer with 0.1 mm thickness. Within a unit cell, the adjacent grid spacing g = 3.2 mm. Ceramics and copper are built on a low-loss quartz substrate with a relative permittivity of 3.9 and a thickness of d_1 = 6 mm. A low-permittivity FR4 dielectric layer, with a thickness of $d_2 = 1/2\ a$ = 0.9 mm, is inserted between the metallic structure and the substrate, leaving a square hole at the center for ceramic particle placement. The periodicity p of the unit cell is 6 mm. The structure is designed with four-fold rotational symmetry in the xOy plane, ensuring polarization-independent response for TE and TM modes.

The fabrication of the metamaterial sample comprises three main parts. First, $SrTiO_3$ bulk ceramic was

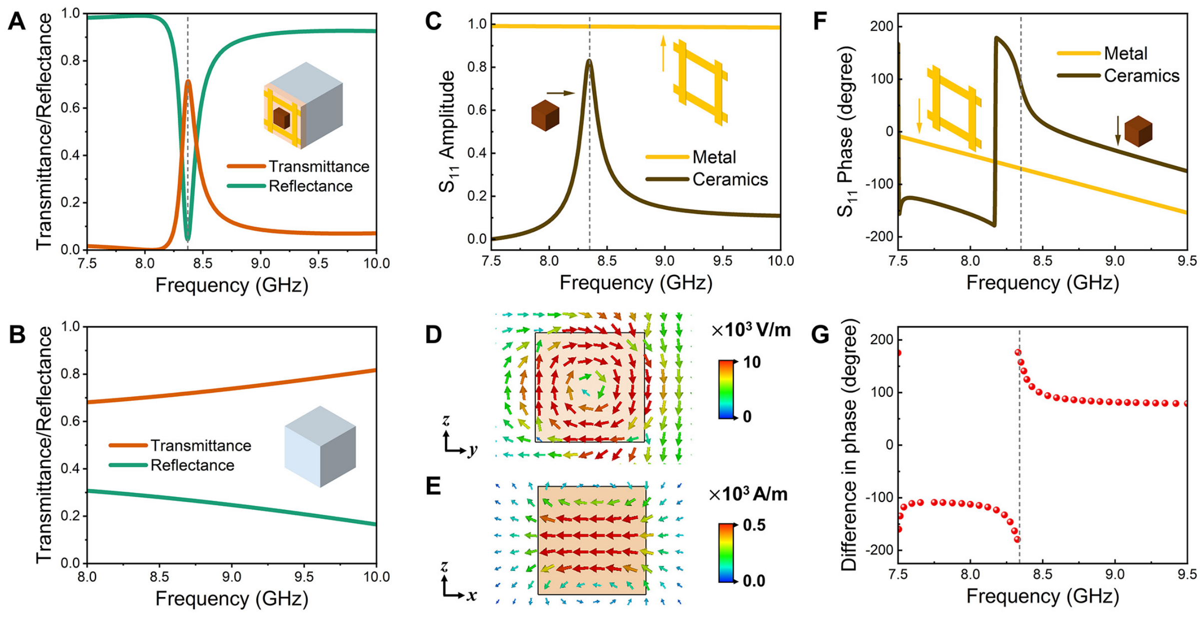

Figure 2. (A) Simulated transmittance and reflectance spectra of the metamaterial. (B) Simulated transmittance and reflectance spectra of the quartz substrate. (C) Simulated S_{11} amplitudes of the ceramic particle array and metallic grid array individually. (D) Electric field distribution of ceramic particle in the *yOz* plane. (E) Magnetic field distribution of ceramic particle in the *xOz* plane. (F) Simulated S_{11} phases of the ceramic particle array and metallic grid array individually. (G) Difference in the S_{11} phase between the ceramic particle array and the metallic grid array.

processed into specific-sized particles through steps including slicing, grinding, and dicing. Subsequently, the FR4 dielectric plate was machined with 1.8 mm × 1.8 mm square holes for the placement of ceramic particles. The crisscrossing metal grids were patterned on both sides of the copper-clad PI film through photolithography and etching, and the square holes of the same size were then machined into the structure. FR4 dielectric plate, metal grids on PI film, and the $SrTiO_3$ ceramic particles were all manually adhered to the quartz substrate with PI tape. The experimental measurement was carried out via a free-space transmission measurement system. Meanwhile, a vector network analyzer, a multi-channel thermocouple, an infrared thermal imager, and a stopwatch were also used to acquire transmittance spectra, temperature, and modulation time results, respectively.

RESULTS AND DISCUSSION

High-transmission mechanism

For the designed metamaterial, the electromagnetic response was numerically simulated in CST Microwave Studio. The propagation of the incident electromagnetic wave was along the *z*-axis, and the electric field and magnetic field were polarized along the *y*- and *x*-axes, respectively. As evidenced in Figure 2A, the metamaterial exhibits a selective high-transmission response at 8.37 GHz, with a transmittance $T = |S_{21}|^2 = 0.71$, accompanied by suppressed reflectance ($R = |S_{11}|^2$) less than 0.05. Figure 2B demonstrates the transmittance and reflectance spectra of the quartz with a thickness of 6 mm. In 8-10 GHz, the quartz exhibits no resonant behavior and maintains high transmission characteristics, with a transmittance of $T = 0.70$ at 8.37 GHz. It indicates that the addition of the metallic grid array and the ceramic particle array has almost no effect on the transmission features of the quartz substrate at this frequency. Based on the selective high transmission, this metamaterial can be used as frequency selective surfaces (FSSs) and band-pass filters.

The comprehensive analysis demonstrates that the selective high transmittance arises from the dispersion tailoring of the incident field at the metamaterial interface, facilitated by the ceramic particle array and metallic grid structures. When analyzing these components separately under the identical periodic arrangement, both of them inherently behave as reflectors. As shown in Figure 2C, at 8.35 GHz, the S_{11} amplitudes for the ceramic particle array and the metallic grids are 0.83 and 0.99, respectively. The abrupt change in S_{11} of the ceramic particle array is attributed to Mie resonance. At 8.35 GHz, first-order Mie resonance occurs in the ceramic particle array, which behaves as a magnetic dipole (MD). Figure 2D and E illustrate this phenomenon through field distributions of the circular electric field in the *yOz* plane and the transverse magnetic field in the *xOz* plane. After combining the ceramic particle together with metallic grid, the overall structure exhibits high transparency, which is contributed to the destructive interference of two reflected waves. The S_{11} phases of the ceramic particle array and the metallic grid array are shown in Figure 2F, and the phase difference is depicted in Figure 2G. It can be observed that there is precisely 180° phase disparity at 8.35 GHz. Through comparative analysis of Figure 2C and F, the two reflected electromagnetic waves basically meet the conditions for destructive interference near 8.35 GHz, which leads to high transmission performance, verifying the conceptual illustration in Figure 1A.

Electrically tunable mechanism

To verify the temperature-dependent characteristics of permittivity in Equation (4), we fabricated a $SrTiO_3$ specimen and measured the variation of its permittivity with temperature, as shown in Figure 3A. At room temperature, the measured real part of the relative permittivity of this ceramic is 325. This value exhibited approximately linear degradation with increasing temperature, declining to 234 at 200 °C. Furthermore, to experimentally validate the aforementioned temperature-dependent Mie resonant frequency of the ceramic particle, we cut the above-mentioned ceramic into cuboid particles (2.4 mm × 2.4 mm × 2.9 mm), and fixed them to the center of the WR-90 waveguide with polyimide tape. The side with a length of 2.9 mm was placed along the direction of electromagnetic wave propagation, and the thermal tuning of resonant frequencies was measured. As demonstrated in Figure 3B, with temperature increasing, the ceramic particle resonated at higher frequencies. Due to technical limitations, the calibration of the measurement was completed at room temperature. However, the waveguide will deform at high temperatures, leading to calibration errors that cause the transmittance measured at 200 °C to be slightly higher than 1 at lower frequencies. Nevertheless, this figure is still persuasive for drawing qualitative conclusions about the dependent relationship between the resonant frequencies of ceramic particles and the temperatures.

Correspondingly, the transmission peak frequency of the metamaterial also varies with temperature. Using Equation (4) and taking the ceramic relative permittivity of 280 at room temperature (25 °C) as the baseline for simulation parameters, the relative permittivity at temperatures from 20 to 120 °C was calculated and the simulated transmittance spectra of the metamaterial were shown in Figure 3C. The temperature-sensitive transmission property of this metamaterial is verified. Furthermore, to evaluate the changing rate of transmission peak frequency with temperature increase, we derived the data from Figure 3C and plotted the frequency variation (ΔFrequency) as a function of temperature variation (ΔTemperature) in Figure 3D. Here, the ΔTemperature is defined as the difference between the stable temperature and the initial room temperature, while ΔFrequency represents the change in the transmittance peak frequency between these two temperatures. According to the curve fitting results, the shift of transmission peak frequency exhibits an approximately linear relationship with temperature elevation, demonstrating an average shift rate of 0.011 GHz/°C.

Dynamically tunable results

Figure 4A presents a photograph of the fabricated prototype, which has an overall size of 200 mm × 200 mm. The red wire in the top-right corner of the photograph was used to connect to an external stabilized voltage supply, enabling the application of voltages. Figure 4B displays the measured transmittance spectra of the

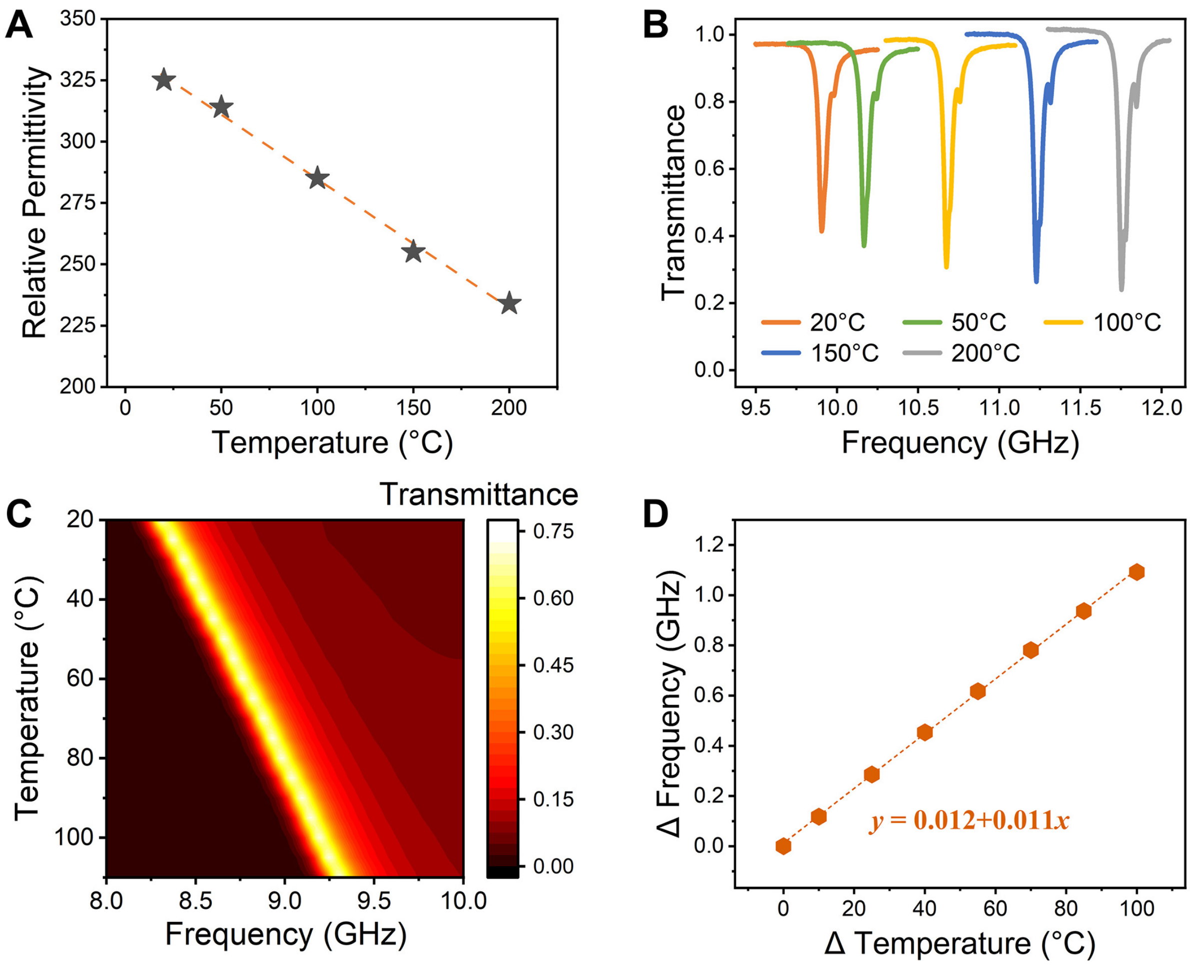

Figure 3. (A) Dependence of measured relative permittivity of $SrTiO_3$ on different temperatures. (B) Measured transmittance spectra of the $SrTiO_3$ particle array with the size of 2.4 mm × 2.4 mm × 2.9 mm. (C) Simulation transmittance of the metamaterial with temperature changing from 20 to 120 °C. (D) Simulation transmission peak frequency shift range (ΔFrequency) with the increment of temperature (ΔTemperature) and corresponding curve fitting results (dashed line).

metamaterial at different temperatures (voltages). At room temperature, the metamaterial achieves a selective high transmittance of 0.81 at 8.07 GHz. Due to the preparation errors, the actual relative permittivity of $SrTiO_3$ ceramic is 292. After adjusting the simulation parameters, the simulation results are in reasonable agreement with the experimental results, as shown in the inset of Figure 4B. Compared to the simulation results, the experimental results observed more oscillating peaks due to the processing errors in the ceramic particles. Since the sizes of some particles may deviate from designed values, the metamaterial sample cannot resonate at a single unified frequency, resulting in additional transmission peaks.

To achieve different temperature increments, voltages of 10, 15, 20, and 25 V were applied. We performed the temperature measurements when the data displayed on the vector network analyzer ceased to fluctuate. Since the metamaterial sample was in direct contact with the air, non-uniform heating was observed during the process of applying voltages [Supplementary Figure 1]. Therefore, the central area of the metamaterial sample, which was aligned with the lens antenna, was selected as the temperature measurement region. Future work could mitigate this non-uniform heating through structural optimization, such as reducing the spacing between metal grids and between metal grids and ceramic particles, and adopting substrates with higher thermal conductivity. Additionally, transferring the experimental measurement to a thermal insulation system would also minimize temperature differences between the metamaterial and surroundings.

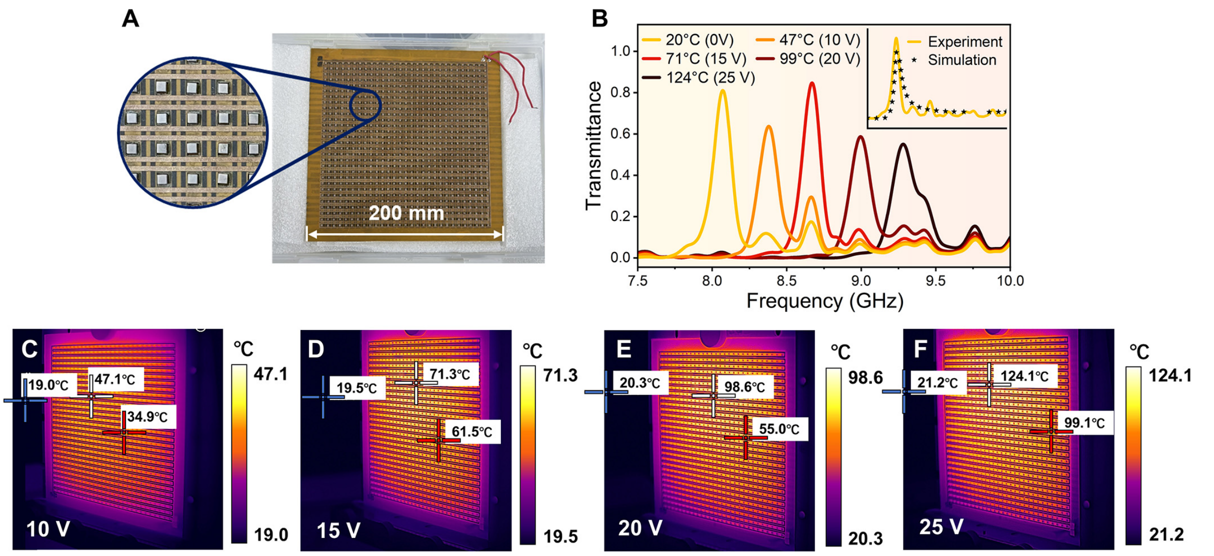

Figure 4. (A) Photograph of the metamaterial sample. (B) Demonstration of measured electrically tunable transmittance spectra at different temperatures (voltages). (Inset: consistent transmittance spectra of experimental results and simulation results at room temperature). Infrared thermography of the stabilized temperature field distribution under (C) 10 V, (D) 15 V, (E) 20 V, and (F) 25 V.

According to the infrared thermography results, the stable temperatures corresponding to the different voltages were 47, 71, 99, and 124 °C, as shown in Figure 4C-F. It can be observed from Figure 4B that an increase in temperature causes the transmission peak to shift toward higher frequencies. As the voltage increases from 10 to 25 V, the stable transmission peak shifts from 8.07 to 9.28 GHz, achieving a modulation frequency range of 1.21 GHz. Additionally, during the heating process, the metamaterial maintains stable high transmittance characteristics (~ 0.6), with the maximum transmittance T_{max} = 0.85 observed at 15 V. At voltages of 20 and 25 V, the maximum transmittance slightly decreases. For $SrTiO_3$ ceramics, research indicates that the relationship between dielectric loss and temperature follows $(T - T_c)\tan\delta = \alpha + \beta T + \gamma T^2$[23], where T_c represents the Curie temperature of the material and α, β, and γ are parameters unrelated to the temperature. Within the temperature range of 20-150 °C, which is the focus of our study, the dielectric loss increases slightly with rising temperature, but the variation does not exceed 1×10^{-4}. Supplementary Figure 2 demonstrates that as the dielectric loss of the ceramic material increases, the maximum transmittance of the metamaterial decreases, while the impact on the transmittance in non-transmission bands is negligible. Therefore, the transmission performance of the metamaterial is minimally affected by $\tan\delta$ of ceramic material as temperature increases. Consequently, when applying voltages of 20 and 25 V, the maximum transmittance of the metamaterial decreases due to a larger temperature difference between the metamaterial sample and the environment, which causes ceramic particles at different positions to be unable to maintain uniform permittivity and resonance frequencies.

For a more accurate and systematic analysis of the transmittance modulation process, the concept of modulation depth P is introduced as follows. For the process where the transmittance increases from minimum to maximum:

$$P = \frac{T - T_{\min}}{T_{\max} - T_{\min}} \times 100\% \tag{5}$$

and for the process where the transmittance decreases from maximum to minimum:

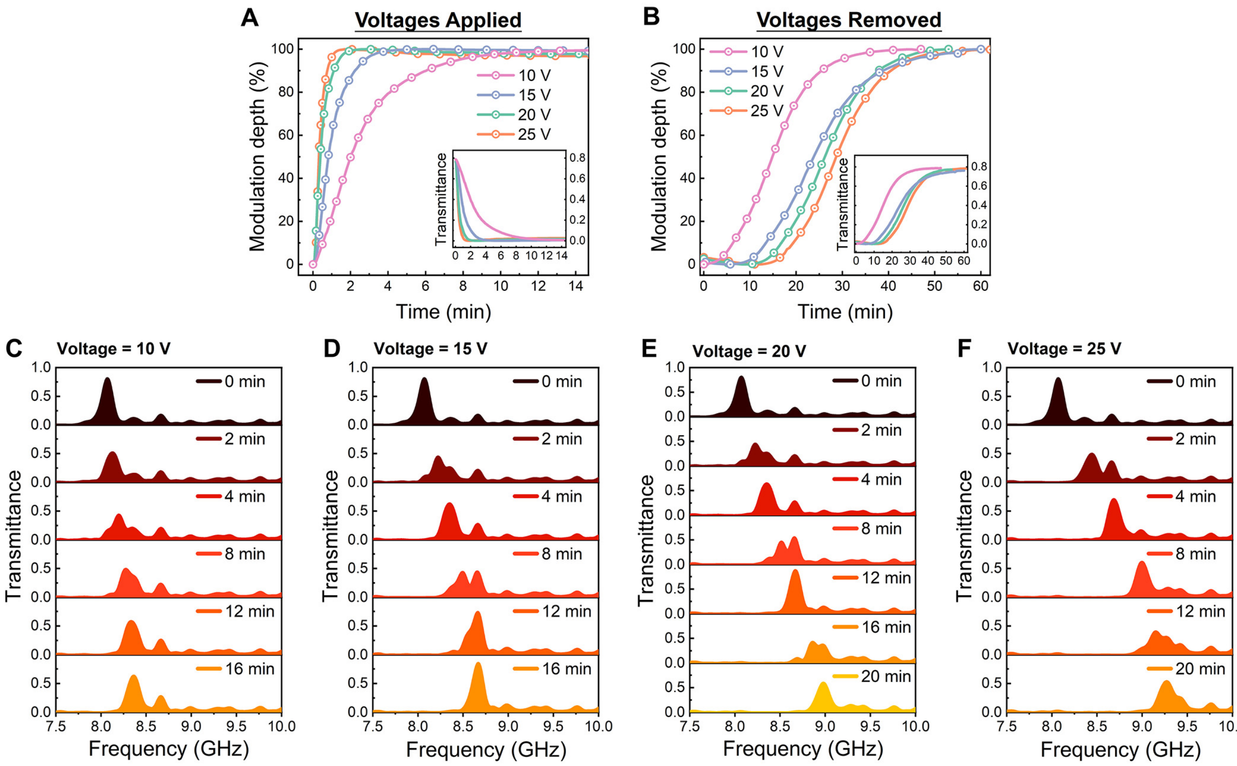

Figure 5. Modulation depth of 8.07 GHz during the process of (A) voltages applied and (B) voltages removed. (Inset: variation of transmittance with time). Demonstration of the dynamic modulation process with voltages of (C) 10 V, (D) 15 V, (E) 20 V, and (F) 25 V.

$$P = \frac{T_{\max} - T}{T_{\max} - T_{\min}} \times 100\% \tag{6}$$

In both equations, T_{max} and T_{min} represent the maximum and the minimum transmittance achievable during the entire modulation process at the given frequency, and T represents the transmittance at the moment to be calculated. At 8.07 GHz, during the heating process at different voltages, transmittance decreases at varying speeds from its maximum to a lower level (as shown in the inset of Figure 5A). The modulation depth as a function of time is shown in Figure 5A, indicating that the higher the voltage, the faster the modulation rate. The fastest modulation depth for P = 90% can be achieved in 0.83 min at the voltage of 25 V, where the transmittance drops from 0.81 to 0.06. Once the voltage is removed, a reverse modulation process occurs, where the transmittance at 8.07 GHz will rise back to the maximum under different modulation rates. Under lower voltages, a narrower modulation frequency range is obtained, which enables an accelerated modulation speed for transmittance at 8.07 GHz to rise toward the transmission peak, as demonstrated in Figure 5B. Due to the thermal hysteresis arising from the non-instantaneous generation and conduction of Joule heat, and the fact that forming a stable transmission response in the metamaterial requires a certain duration [Supplementary Figure 1], the current metamaterial and its electrical tuning method exhibit certain limitations for rapid-response applications.

Figure 5C-F show the dynamic process of transmittance over time at different voltages. For analytical simplicity, the application of 10 V voltage is selected for discussion, and the modulation processes of other voltages are similar. During the process of applying voltage, the high-transmission property at room temperature becomes unstable. The transmittance at 8.07 GHz decreases, and there is a shift toward higher frequency. Eventually, the transmission peak stabilizes at 8.38 GHz, resulting in a frequency shift of 0.31 GHz. When comparing the electrically tuning results at different voltages, a positive correlation is

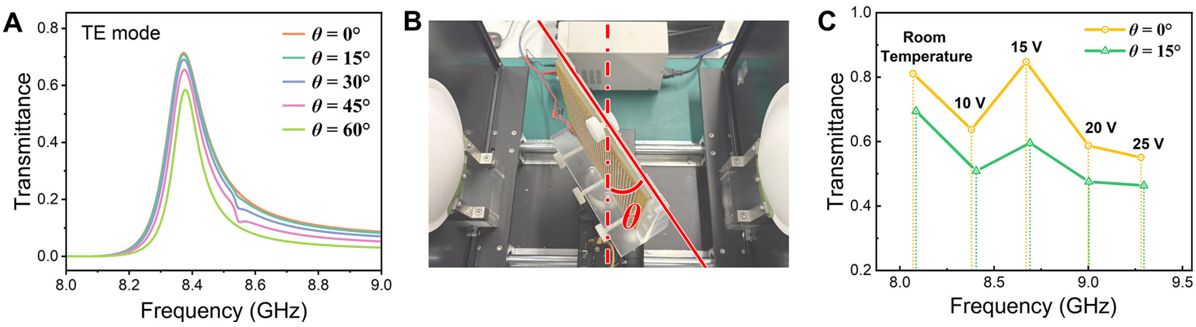

Figure 6. (A) Simulated transmittance spectra of TE-polarized wave under the oblique incidence of 0-60°. (B) Oblique incidence experimental setup. (C) Measured transmittance modulation results (containing maximum transmittance and transmission peak frequency) for normal and oblique incidence.

observed between the modulation frequency range and the temperature variation (ΔTemperature), where ΔTemperature is defined the same as that in MATERIALS AND METHODS. Each ΔTemperature for four voltages is 27.4, 51.7, 79.5, and 104.5 °C, corresponding to the frequency shift of 0.31, 0.60, 0.93, and 1.21 GHz, respectively. By performing curve fitting on the above data, the measured average transmission peak frequency shift rate is 0.0117 GHz/°C, demonstrating a high agreement between the measurement results and the simulations.

Moreover, we also focused on the oblique incidence characteristics. The simulated transmittance of TE-polarized waves under oblique incidence within 0-60° is shown in Figure 6A. Due to the impedance characteristics of TE mode, the transmittance decreases with increasing incident angle. Since the metamaterial sample is not large enough for the lens antenna, large-angle oblique incidence measurement is not suitable for this work. Therefore, the case of an oblique incidence angle θ = 15° is selected for the experiment, and the schematic diagram of the rotation of the sample holder is shown in Figure 6B. Similarly, voltages of 10, 15, 20, and 25 V are applied, and the different electrical modulation results are plotted in Figure 6C. When electromagnetic waves are incident obliquely, transmission peak frequencies at different voltages remain unchanged and the transmittance maximum decreases, which is consistent with the simulation results. However, the measured transmittance maximum exhibits more significant degradation with the increasing incident angle. This discrepancy arises from fabrication errors, where the precision cutting of cubic ceramic particles and the assembly process could both introduce structural deviations from theoretical models. These imperfections lead to enhanced anisotropy of the metamaterial sample, thereby amplifying the disparity in transmissive characteristics between normal and oblique incidence conditions. Future work will prioritize the fabrication of scaled-up metamaterial samples to enable wide-angle measurements under identical systems. This will enhance comparisons with simulation results at wider incidence angles (±60°) and facilitate systematic analysis of how oblique incidence angles affect the transmission performance of the metamaterial.

To demonstrate the exceptional tuning performance of the metamaterial, we compare it with four typical types of electrically tunable metamaterials: graphene-based, varactor diode-based, liquid crystal-based, and BST ceramic-based. Their maximum voltage application, frequency shift ranges, and basic tunable performance are summarized in Table 1.

The graphene-based and liquid crystal-based metamaterials listed are applied in the THz band, so we focus on comparing voltage requirements and tunable performance. In our work, a transmittance variation of nearly 80% is achieved with an applied voltage of only 25 V, while the former ones exhibit relatively small

Table 1. Summary of several electrically tunable metamaterials

Metamaterial types	Maximum voltage	Frequency/Wavelength shift range	Tunable performance (variation of reflectance/transmittance)
Graphene[24]	80 V	~ 1 μm	Reflectance: modulation depth* of 95% at 6 μm, with a variation of about 45%
Liquid Crystal[25]	300 V	0.7-1.1 THz	Transmittance: variation of 19% at 1 THz
Varactor Diode[26]	12 V	5.18-5.68 GHz	Reflectance: variation of 90.5% at 5.68 GHz
Varactor Diode[27]	8 V	3.11-3.27 GHz	Transmittance: variation of 57.5% at 3.11 GHz
BST ceramic[15]	~ 300 V	9.5-10.5 GHz	Phase manipulation
This work	25 V	8.07-9.28 GHz	Transmittance: variation of 78.3% (from 81% to 2.7%) at 8.07 GHz

*Modulation depth in this table is calculated by 1 - (R_{min}/R_{max}), where R_{max} and R_{min} are the maximum and minimum achievable reflectance for the specific wavelength.

changes in reflectance or transmittance. Varactor-diode-based tunability offers operational convenience with low voltage requirements. Due to the cutoff frequency limitation, this kind of metamaterial is mainly applied in the microwave band, which is comparable in range to our work. The frequency shift range reported in the listed studies does not exceed 0.5 GHz, whereas our design achieves a shift of up to 1.21 GHz. Additionally, metamaterials employing BST ceramics - which have electric field-dependent permittivity - can also enable tunability, but this method requires an excessively large electric field (estimated at ~kV/cm), which is less convenient for experimental operation compared to our design. In summary, the metamaterial designed in this work demonstrates comprehensive performance across multiple tunable indicators.

CONCLUSIONS

In conclusion, we have demonstrated a transmissive dielectric metamaterial composed of periodic $SrTiO_3$ Mie resonators and metallic grid arrays, capable of electrically tunable electromagnetic responses in the microwave frequency range. By leveraging destructive interference between reflected waves from two scattering bodies, the metamaterial achieves selective high transmission. The temperature-dependent permittivity of the ceramic material enables voltage application to the metallic grid, where the thermal effect of the current heats the ceramic particles. This leads to a frequency shift of both the Mie resonance and the transmission peak, enabling dynamical electrical tunability of the metamaterial's electromagnetic properties. Upon applying an external voltage of 25 V, the microwave transmission was modulated by 0.75 with a frequency shift of 1.21 GHz in less than one minute. This approach paves a promising path for the development of active microwave windows with exceptional performances and scalability, holding significant potential for applications in wireless communications, radar, and other microwave systems.

DECLARATIONS

Authors' contributions

Conception and experimental design, data interpretation: Liu, L.; Wang, X.
Data acquisition and analysis: Liu, L.; Wang, X.; Wang, Y.; Zhao, R.; Jin, Y.
Manuscript writing and revision: Liu, L.; Wang, X.; Wen, Y.
Supervision: Li, B.; Wen, Y.; Zhou, J.

Availability of data and materials

The data that support the findings of this study are available from the corresponding author upon reasonable request.

Financial support and sponsorship

This work was supported by the National Key R&D Program of China (2022YFB3806000), the Basic Science Center Project of NSFC (52388201), National Natural Science Foundation of China (52332006), and Beijing Natural Science Foundation (Z240008).

Conflicts of interest

All authors declared that there are no conflicts of interest.

Ethical approval and consent to participate

Not applicable.

Consent for publication

Not applicable.

Copyright

Supplementary Materials

Supplementary Materials

REFERENCES

1. Kim, J.; Kim, B.; Kim, B.; Jeon, H.; Kim, S. K. Magnetic-field controlled on-off switchable non-reciprocal negative refractive index in non-Hermitian photon-magnon hybrid systems. *Nat. Commun.* **2024**, *15*, 9014. DOI PubMed PMC
2. Liu, Y.; Dong, T.; Qin, X.; et al. High-permittivity ceramics enabled highly homogeneous zero-index metamaterials for high-directivity antennas and beyond. *eLight* **2024**, *4*, 59. DOI
3. Wen, Y.; Zhou, J. Artificial nonlinearity generated from electromagnetic coupling metamolecule. *Phys. Rev. Lett.* **2017**, *118*, 167401. DOI
4. Qin, H.; Su, Z.; Zhang, Z.; et al. Disorder-assisted real-momentum topological photonic crystal. *Nature* **2025**, *639*, 602-8. DOI
5. Wang, J.; Weber, T.; Aigner, A.; Maier, S. A.; Tittl, A. Mirror-coupled plasmonic bound states in the continuum for tunable perfect absorption. *Laser. Photon. Rev.* **2023**, *17*, 2300294. DOI
6. Landy, N. I.; Sajuyigbe, S.; Mock, J. J.; Smith, D. R.; Padilla, W. J. Perfect metamaterial absorber. *Phys. Rev. Lett.* **2008**, *100*, 207402. DOI PubMed
7. Soric, J.; Ra'di, Y.; Farfan, D.; Alù, A. Radio-transparent dipole antenna based on a metasurface cloak. *Nat. Commun.* **2022**, *13*, 1114. DOI PubMed PMC
8. Xu, H. X.; Hu, G.; Wang, Y.; et al. Polarization-insensitive 3D conformal-skin metasurface cloak. *Light. Sci. Appl.* **2021**, *10*, 75. DOI PubMed PMC
9. Yue, Z.; Li, J.; Liu, J.; et al. Versatile polarization conversion and wavefront shaping based on fully phase-modulated metasurface with complex amplitude modulation. *Adv. Opt. Mater.* **2022**, *10*, 2200733. DOI
10. Zhao, Q.; Du, B.; Kang, L.; et al. Tunable negative permeability in an isotropic dielectric composite. *Appl. Phys. Lett.* **2008**, *92*, 051106. DOI
11. Wang, X.; Zhou, J. Fano resonance in a subwavelength Mie-based metamolecule with split ring resonator. *Appl. Phys. Lett.* **2017**, *110*, 254101. DOI
12. Li, R.; Xu, D.; Avdeev, M.; et al. Ultralow loss and high tunability in a non-perovskite relaxor ferroelectric. *Adv. Funct. Mater.* **2023**, *33*, 2210709. DOI
13. Sun, X.; Fu, Q.; Fan, Y.; et al. Thermally controllable Mie resonances in a water-based metamaterial. *Sci. Rep.* **2019**, *9*, 5417. DOI PubMed PMC
14. Wang, Q.; Zeng, L.; Lei, M.; Bi, K. Tunable metamaterial bandstop filter based on ferromagnetic resonance. *AIP. Adv.* **2015**, *5*, 077145. DOI
15. Su, Z.; Zhao, Q.; Song, K.; Zhao, X.; Yin, J. Electrically tunable metasurface based on Mie-type dielectric resonators. *Sci. Rep.* **2017**, *7*, 43026. DOI PubMed PMC
16. Weigand, H. C.; Talts, ÜL.; Vieli, A. L.; Vogler-Neuling, V. V.; Nardi, A.; Grange, R. Nanoimprinting solution-derived barium titanate for electro-optic metasurfaces. *Nano. Lett.* **2024**, *24*, 5536-42. DOI PubMed PMC
17. Karvounis, A.; Vogler-Neuling, V. V.; Richter, F. U.; Dénervaud, E.; Timofeeva, M.; Grange, R. Electro-optic metasurfaces based on barium titanate nanoparticle films. *Adv. Opt. Mater.* **2020**, *8*, 2000623. DOI
18. Liu, X.; Ren, Z.; Yang, T.; Chen, L.; Wang, Q.; Zhou, J. Tunable metamaterial absorber based on resonant strontium titanate artificial atoms. *J. Mater. Sci. Technol.* **2021**, *62*, 249-53. DOI
19. Zhao, Y.; Li, B.; Lan, C.; Bi, K.; Qu, Z. Tunable silicon-based all-dielectric metamaterials with strontium titanate thin film in terahertz range. *Opt. Express.* **2017**, *25*, 22158-63. DOI

20. He, X.; Lin, F.; Liu, F.; Shi, W. Tunable strontium titanate terahertz all-dielectric metamaterials. *J. Phys. D. Appl. Phys.* **2020**, *53*, 155105. DOI
21. Lewin, L. The electrical constants of a material loaded with spherical particles. *J. Inst. Electr. Eng.* **1947**, *94*, 65-8. DOI
22. Kell, R. C.; Greenham, A. C.; Olds, G. C. E. High-permittivity temperature-stable ceramic dielectrics with low microwave loss. *J. Am. Ceram. Soc.* **1973**, *56*, 352-4. DOI
23. Rupprecht, G.; Bell, R. O. Microwave losses in strontium titanate above the phase transition. *Phys. Rev.* **1962**, *125*, 1915-20. DOI
24. Yao, Y.; Shankar, R.; Kats, M. A.; et al. Electrically tunable metasurface perfect absorbers for ultrathin mid-infrared optical modulators. *Nano. Lett.* **2014**, *14*, 6526-32. DOI
25. Kowerdziej, R.; Olifierczuk, M.; Parka, J.; Wróbel, J. Terahertz characterization of tunable metamaterial based on electrically controlled nematic liquid crystal. *Appl. Phys. Lett.* **2014**, *105*, 022908. DOI
26. Zhu, J.; Li, D.; Yan, S.; Cai, Y.; Liu, Q. H.; Lin, T. Tunable microwave metamaterial absorbers using varactor-loaded split loops. *Europhys. Lett.* **2015**, *112*, 54002. DOI
27. Fu, Q.; Zhang, F.; Fan, Y.; He, X.; Qiao, T.; Kong, B. Electrically tunable Fano-type resonance of an asymmetric metal wire pair. *Opt. Express.* **2016**, *24*, 11708-15. DOI